# Berry phase jumps and giant nonreciprocity in Dirac quantum dots

Joaquin F. Rodriguez-Nieva and Leonid S. Levitov

Phys. Rev. B **94**, 235406 — Published 6 December 2016

DOI: 10.1103/PhysRevB.94.235406

# Berry phase jumps and giant non-reciprocity in Dirac quantum dots

Joaquin F. Rodriguez-Nieva and Leonid S. Levitov
*Department of Physics, Massachusetts Institute of Technology, Cambridge, MA 02139, USA*

We predict strong non-reciprocity in the resonance spectra of Dirac quantum dots induced by the Berry phase. The non-reciprocity arises in relatively weak magnetic fields and is manifest in anomalously large field-induced splittings of quantum dot resonances which are degenerate at $B = 0$ due to time-reversal symmetry. This exotic behavior is unique to quantum dots in Dirac materials and is absent in conventional quantum dots. The effect, which is governed by field-induced jumps in the Berry phase of confined electronic states, is strong for gapless Dirac particles and can overwhelm the $B$-induced orbital and Zeeman splittings. A finite Dirac mass suppresses the effect. The non-reciprocity, predicted for a large family of two-dimensional Dirac materials, is accessible via Faraday and Kerr optical rotation measurements and scanning tunneling spectroscopy.

## I. INTRODUCTION

Recently, a new class of quantum dots embedded in two-dimensional Dirac materials has been introduced[1]. The Dirac quantum dots are defined by nanoscale $p$-$n$-junction rings induced by electrostatic potentials, with Klein scattering at the p-n junctions serving as a vehicle for confinement of electronic states[2–7]. Carrier confinement in these ring-shaped electron resonators arises due to constructive interference of electronic waves scattered at the $pn$ junction[8, 9] and inward-reflected from the ring. Confined states are manifest through resonances appearing periodically in scanning tunneling spectroscopy maps[1]. Here we show that this mechanism for electronic confinement can be exploited for accessing exotic and potentially useful behavior which is not available in conventional quantum dots.

In particular, we predict that the Berry phase, a signature topological characteristic of Dirac materials[10–16], induces a strongly non-reciprocal effect of quantum dot resonances,

$$\varepsilon_{n,m} \neq \varepsilon_{n,-m}, \tag{1}$$

in the presence of a weak magnetic field $B$; here $m$ and $n$ denote the azimuthal and radial quantum numbers, respectively (for optical non-reciprocity, see Refs.[17, 18]). As we will see, resonance splittings of the $\pm m$ states, which are degenerate at $B = 0$, grow rapidly with magnetic field, approaching values as large as half the quantum dot resonance period $\Delta\varepsilon$. In particular, for the weak $B$ of interest, the effect dominates over the $B$-induced orbital and Zeeman splittings.

## II. SEMICLASSICAL DESCRIPTION

This anomalous behavior can be understood from a simple semiclassical picture describing confined electrons in a gapless two-band system. Considering a confining potential with circular symmetry, the resonance spectrum $\varepsilon_{n,m}$ of the quantum dot can be obtained from the WKB condition for $\varphi_{\rm orb} = \frac{1}{\hbar}\oint_{\mathcal{C}} d\boldsymbol{r}\cdot\boldsymbol{p}$, the usual orbital phase accumulated along the classical path $\mathcal{C}$:

$$\varphi_{\rm orb}(\varepsilon, m) + \varphi_{\rm B}(\varepsilon, m) = 2\pi(n+\gamma), \tag{2}$$

where $\varphi_{\rm B}$ is Berry phase and $\gamma$ a constant[11, 15, 19]. The Dirac bandstructure gives rise to a geometric gauge field that generates the Berry phase,

$$\varphi_{\rm B} = \oint_{\mathcal{C}} d\boldsymbol{h}\cdot\langle \boldsymbol{h}_+|i\nabla_{\boldsymbol{h}}|\boldsymbol{h}_+\rangle = S(\mathcal{C})/2. \tag{3}$$

In Eq.(3), $S(\mathcal{C})$ denotes the solid angle subtended by the vector $\boldsymbol{h} = (h_x, h_y, h_z)$ along a closed path $\mathcal{C}$, with $\boldsymbol{h}$ defined in terms of the two-band Hamiltonian

$$\mathcal{H} = \boldsymbol{\sigma}\cdot\boldsymbol{h} + h_0, \quad \mathcal{H}|\boldsymbol{h}_\pm\rangle = (\pm|\boldsymbol{h}| + h_0)|\boldsymbol{h}_\pm\rangle. \tag{4}$$

Here $h_0$ is a scalar function and $\boldsymbol{\sigma} = (\sigma_x, \sigma_y, \sigma_z)$ are Pauli matrices. The Berry phase in a gapless system ($h_z = 0$) can only take the values $\varphi_{\rm B} = 0$ or $\pm\pi$ [12, 14, 20, 21].

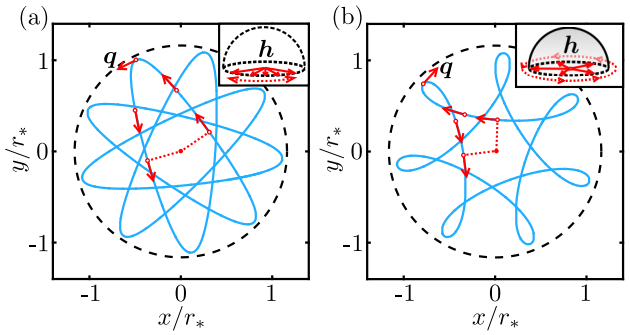


FIG. 1. Control of the Berry phase $\varphi_{\rm B}$ of confined Dirac electrons using magnetic fields. Shown are semiclassical orbits of a massless particle exhibiting topologically distinct orbital behavior corresponding to (a) $B < B_{\rm c}$ and (b) $B > B_{\rm c}$ [see critical field $B_{\rm c}$ in Eq.(7)]. The Berry phase, determined by the solid angle subtended by $\boldsymbol{h} = (h_x, h_y, h_z)$ in Eq.(3), jumps from $\varphi_{\rm B} = 0$ to $\varphi_{\rm B} = \pi$ at $B = B_{\rm c}$, see insets [for gapless systems $h_{x,y} = v\,q_{x,y}$ and $h_z = 0$, with $q_{x,y}$ the kinetic momentum (red vectors) and $v$ the Fermi velocity]. Here we used $m = 1/2$, energy $\varepsilon = 1.35\,\hbar v/r_*$, with $r_*$ defined in Eq.(11), $B/B_{\rm c} = 0.8$ for (a) and $B/B_{\rm c} = 1.6$ for (b).

An external magnetic field has a profound effect on the Berry phase of the orbits, allowing them to switch between the $\varphi_{\rm B} = 0$ and $\pm\pi$ types. As illustrated in Fig.1, switching can take place even in a weak magnetic field. In particular, for $B = 0$ we find $\varphi_{\rm B}(\varepsilon, \pm m) = 0$, whereas for weak nonzero fields we find $\varphi_{\rm B}(\varepsilon, m) = \pi$ and $\varphi_{\rm B}(\varepsilon, -m) = 0$. As a result of the $\pi$ difference in the WKB condition in Eq.(2) for the $\pm m$ states, the $m > 0$ and $m < 0$ families of resonances are shifted by half a period, giving rise to a large resonance splitting (Fig.3):

$$\varepsilon_{n,m} - \varepsilon_{n,-m} \approx \Delta\varepsilon/2, \quad \text{(gapless)} \tag{5}$$

where $\Delta\varepsilon \sim 10{-}50\,$meV is the spacing of resonances in each family. Equation (5) describes gapless Dirac band-structures, a generalization for gapped systems is discussed below.

To illustrate how $B$ controls the Berry phase, we consider a massless particle confined in a radial electrostatic potential $U(r)$. This corresponds to $\boldsymbol{h} = v(q_x, q_y, 0)$ and $h_0 = U(r)$ in Eq.(4). In the presence of a uniform magnetic field $B$, the kinetic momentum $\boldsymbol{q} = \boldsymbol{p} - e\boldsymbol{A}$ is given by

$$\begin{aligned} q_r &= p_r = \pm\sqrt{\left[\varepsilon - U(r)\right]^2/v^2 - (m\hbar/r - eBr/2)^2}, \\ q_\theta &= p_\theta - eA_\theta = m\hbar/r - eBr/2. \end{aligned} \tag{6}$$

Here $v$ is the electron velocity, and we used the axial gauge $A_x = -By/2$, $A_y = Bx/2$ to preserve rotational symmetry. Because the system is integrable, with constants of motion $\varepsilon$ and $m$, we can map $\boldsymbol{q}$ to the surface of a torus. Figure 2 shows such mapping, with $\boldsymbol{q}$ plotted along two curves: $\mathcal{C}_\theta$ in the toroidal direction and $\mathcal{C}_r$ in the poloidal direction. At a critical $B = B_{\rm c}$ we find that the winding number of $\boldsymbol{q}$ along $\mathcal{C}_r$ jumps from 0 to 1, thus resulting in a $\pi$-jump of $\varphi_{\rm B}$.

The semiclassical quantization of quantum dot resonances can now be obtained from Eq.(2) using $\boldsymbol{q}$ in Eq.(6) evaluated on both $\mathcal{C} = \mathcal{C}_\theta$ and $\mathcal{C} = \mathcal{C}_r$ [22]. This yields two quantization conditions for $m$ and $\varepsilon$. For $\mathcal{C} = \mathcal{C}_\theta$, Eq.(2) yields $m = n_\theta + \gamma_\theta - \varphi_{\rm B}/2\pi$, where $\varphi_{\rm B} = \pi$ independently of $B$ [see blue curves in panels (b) and (c) of Fig.2]. Using $\gamma_\theta = 0$, we find the anticipated quantization of angular momentum $m$=half–integer. For $\mathcal{C} = \mathcal{C}_r$, instead, we find $\frac{1}{\hbar}\int_{r_1}^{r_2} dr\, p_r = 2\pi(n_r + \gamma_r) - \varphi_{\rm B}$, where $r_1$ and $r_2$ are the classical return points. The half period shift in the radial quantization condition results from the $\pi$-jump in $\varphi_{\rm B}$ at $B = B_{\rm c}$.

While the same semiclassical picture applies to gapped Dirac systems ($h_z \neq 0$), there are important differences with respect to the gapless case. In particular, the solid angle subtended by the vector $\boldsymbol{h}$, which now points towards the upper hemisphere, is strictly smaller than $2\pi$; non-reciprocity induced by Berry phase is quenched at increasing bandgaps, as will be shown with a more detailed quantum model in Fig.4. In the limit $|h_z| \gg |h_{x,y}|$, orbital splitting dominates.

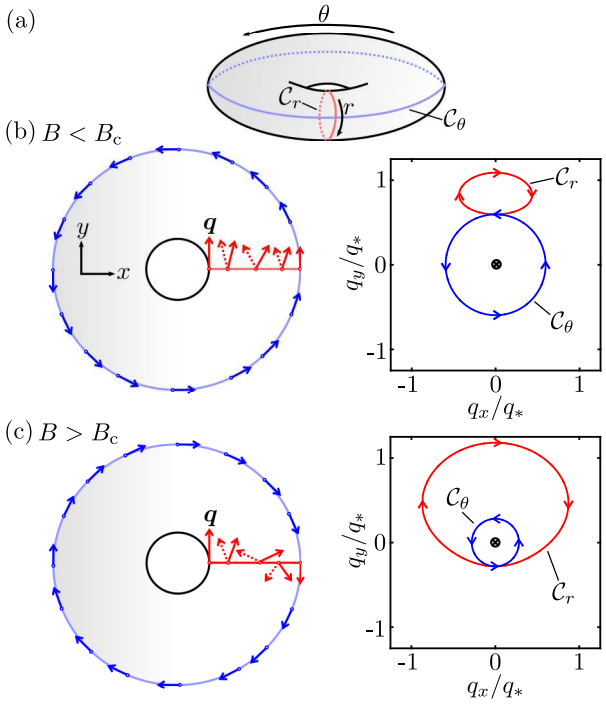


FIG. 2. Topologically distinct mappings of $\boldsymbol{q}$ [Eq.(6)] to the surface of a torus (a), plotted for (b) $B < B_{\rm c}$ and (c) $B > B_{\rm c}$. Indicated with blue(red) arrows is $\boldsymbol{q}$ along the curves $\mathcal{C}_\theta(\mathcal{C}_r)$ shown in panel (a), where dotted lines/arrows indicate a curve/vector in the bottom surface of the torus. At $B = B_{\rm c}$, there is a transition between trivial and non-trivial winding of $\boldsymbol{q}$ along $\mathcal{C}_r$. This results in $B$-induced phase jumps of the Berry phase. Here we define $q_* = \varepsilon_*/v$ and use the same parameter values as in Fig.1.

The jump in Berry phase corresponds to a transition from convex orbits to skipping orbits (Fig.1). This observation allows to define the critical field $B_{\rm c}$ that induces giant non-reciprocity, i.e. the field necessary to reverse the electron velocity at the outer classical return point. From Eq.(6) we find $q_\theta = m\hbar/r_2(\varepsilon) - eB_{\rm c}r_2(\varepsilon)/2 = 0$, with $r_2(\varepsilon)$ the outer return point [i.e. $q_r(r_2) = 0$]. For a quadratic potential model $U(r) = \kappa r^2$, this condition yields

$$B_{\rm c}[{\rm T}] = \frac{2\hbar m\kappa}{e\varepsilon} = 1.3\,\frac{m\kappa[{\rm eV}/\mu{\rm m}^2]}{\varepsilon[{\rm meV}]}. \tag{7}$$

Using typical values obtained in recent experiments[1], $\kappa \approx 4\,{\rm eV}/\mu{\rm m}^2$, $\varepsilon \approx 10\,$meV and $m = 1/2$, we find $B_{\rm c}$ on the order of $0.3\,$T.

Besides the splitting arising at $B = B_{\rm c}$, another key fingerprint of the non-reciprocal effect is the $m$-dependence of $B_{\rm c}$ exhibited in Eq.(7). This feature can be understood by noticing that, for larger $m$, a larger $B$ is necessary to induce skipping orbits. As we will see, the $m$ dependence of $B_{\rm c}$ gives rise to a peculiar branching pattern of the quantum dot resonances which can be probed in spectral measurements away from the quantum dot center (see Sec.III).

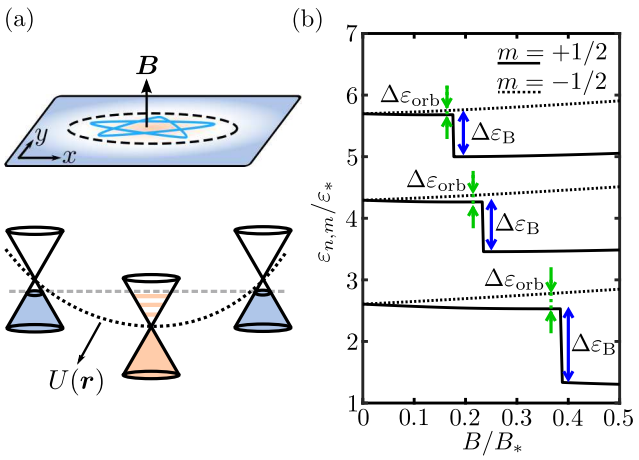


FIG. 3. Magnetic response of quantum dot resonances in a gapless Dirac system. (a) The quantum dot is defined by the circular *pn* ring (dashed lines) induced by a radial electrostatic potential $U(\boldsymbol{r})$. (b) The magnetic response is dominated by the Berry-phase splitting $\Delta\varepsilon_{\rm B}$, which is approximately half the resonance period $\Delta\varepsilon$. Also indicated in the figure is the orbital splitting $\Delta\varepsilon_{\rm orb}$. Peak splitting is calculated from Eq.(2) for $n = 0, 1, 2$, $m = \pm 1/2$, and $\gamma = 0.6$; $B_{\rm c}$ is calculated from Eq.(7); $\varepsilon_*$ and $B_*$ are defined in Eq.(11).

Importantly, the giant non-reciprocal effect relies on the splitting due to Berry phase being dominant over orbital and Zeeman splittings. This is the case, in particular, for the value $B_{\rm c} \sim 0.3\,{\rm T}$ found in Eq.(7). Indeed, $B_{\rm c}$ is significantly lower than the value $B_{\rm LL} = (\Delta\varepsilon)^2/e\hbar v_{\rm F}^2 \sim 1\,{\rm T}$ which is necessary for the first Landau level to be larger than the resonance period $\Delta\varepsilon \approx 25\,{\rm meV}$. The strength of the non-reciprocal effect is illustrated in Fig.3 which shows the semiclassical spectrum obtained from Eq.(2) for $n = 0$ and $m = \pm 1/2$ including both orbital and Berry phase splitting. For typical model parameters, the splitting $\Delta\varepsilon_{\rm B} \sim \Delta\varepsilon/2$ induced by the Berry phase jump dominates over the conventional orbital splitting $\Delta\varepsilon_{\rm orb}$. The effect becomes more dramatic at larger $n$ and smaller $m$. Furthermore, the energy $\varepsilon_{\rm Z}$ for the electron Zeeman splitting, $\varepsilon_{\rm Z} = \mu_{\rm B} B_{\rm c} \sim 10^{-2}\,{\rm meV}$, is negligible compared to the characteristic energy of quantum dots (here $\mu_{\rm B} \approx 5.8 \cdot 10^{-5}\,{\rm eV/T}$ is the Bohr magneton).

## III. MICROSCOPIC MODEL

To contrast the simple semiclassical picture above with a more refined quantum model, we consider the Dirac equation describing confined electrons under the influence of a uniform magnetic field:

$$[v\,\boldsymbol{\sigma}\cdot\boldsymbol{q} + (\Delta/2)\sigma_z + U(\boldsymbol{r})]\,\Psi(\boldsymbol{r}) = \varepsilon\Psi(\boldsymbol{r}). \qquad (8)$$

Here $\Delta$ is the bandgap and $\boldsymbol{q}$ is the kinematic momentum with components $q_{x,y} = -i\hbar\partial_{x,y} - eA_{x,y}$ and $q_z = 0$. This corresponds to $\boldsymbol{h} = v(q_x, q_y, \Delta/2v)$ and $h_0 = U(r)$ in Eq.(4). Because we are interested in eigenstates confined inside the *pn* ring, with radius smaller than the characteristic length of the electrostatic potential, it is legitimate to use a parabolic potential model $U(\boldsymbol{r}) \approx \kappa\boldsymbol{r}^2$. By using the axial gauge $A_x = -By/2$, $A_y = Bx/2$ to preserve rotational symmetry, the eigenstates of Eq.(8) can be expressed using the polar decomposition ansatz,

$$\Psi_m(r,\theta) = \frac{e^{im\theta}}{\sqrt{r}}\begin{pmatrix} u_1(r)e^{-i\theta/2} \\ iu_2(r)e^{i\theta/2}\end{pmatrix}, \qquad (9)$$

with $m$ a half-integer number. This decomposition allows to rewrite Eq.(8) as

$$\begin{pmatrix} r^2 - \varepsilon + \Delta/2 & \partial_r + m/r - Br/2 \\ -\partial_r + m/r - Br/2 & r^2 - \varepsilon - \Delta/2\end{pmatrix}\begin{pmatrix} u_1 \\ u_2\end{pmatrix} = 0. \qquad (10)$$

Here $r$ and $B$ are in units of $r_*$ and $B_*$, respectively, whereas $\varepsilon$ and $\Delta$ are in units of $\varepsilon_*$, with

$$r_* = \sqrt[3]{\hbar v/\kappa} \sim 60\,{\rm nm}, \quad \varepsilon_* = \sqrt[3]{(\hbar v)^2\kappa} \sim 10\,{\rm meV},$$
$$B_* = (\hbar/e)\cdot\sqrt[3]{(\kappa/\hbar v)^2} \sim 0.2\,{\rm T}. \qquad (11)$$

In these estimates, we considered (gapped) graphene $v \approx 10^6\,{\rm m/s}$ as model system and used a typical value of $\kappa = 4\,{\rm eV}/\mu{\rm m}^2$, see estimates below.

A suitable diagnostics of non-reciprocity, allowing direct access to the quantum dot resonances, is the local density of states $D(\varepsilon)$ inside the quantum dot. Naturally, $D(\varepsilon)$ can be obtained experimentally via the $dI/dV$ in STS measurements as in Ref.[1]. The quantity $D(\varepsilon)$ at $r = r_0$ can be conveniently written as the sum of $m$-state contributions $D(\varepsilon) = \sum_m D_m(\varepsilon)$, with

$$D_m(\varepsilon) = \sum_\alpha \langle|u_\alpha(r = r_0)|^2\rangle_{\lambda_d}\delta(\varepsilon - \varepsilon_\alpha). \qquad (12)$$

Here $\alpha$ labels the radial eigenstates of Eq.(10) for fixed $m$, and $\langle|u_\alpha(r = r_0)|^2\rangle_{\lambda_d} = \int_0^\infty dr'|u_\alpha(r')|^2 e^{-(r'-r_0)^2/2\lambda_d^2}$ represents a spatial average of the wavefunction centered at $r = r_0$. A gaussian weight is included in the density of states to account for the finite size of the tunneling region in real STS measurements[1].

### Splitting of quantum dot resonances

Figure 4(a) shows the resulting quantum dot spectrum as a function of $B$ for gapless Dirac systems, exhibiting the $B$-induced splitting of quantum dot resonances. In our calculations, we used $r_0 = 0$, $\lambda_d/r_* = 0.1$, and plotted $\partial D/\partial\varepsilon$ in Eq.(12) in order to enhance spectral features (see Appendix A for details). In agreement with our semiclassical interpretation, a half-period splitting is observed in the gapless spectral maps in Fig.4(a). Because in Fig.4(a) the wavefunction is probed at the center of the quantum dot, only small $m$ states ($m = \pm 1/2$) contribute to the spectral maps. It is important to stress

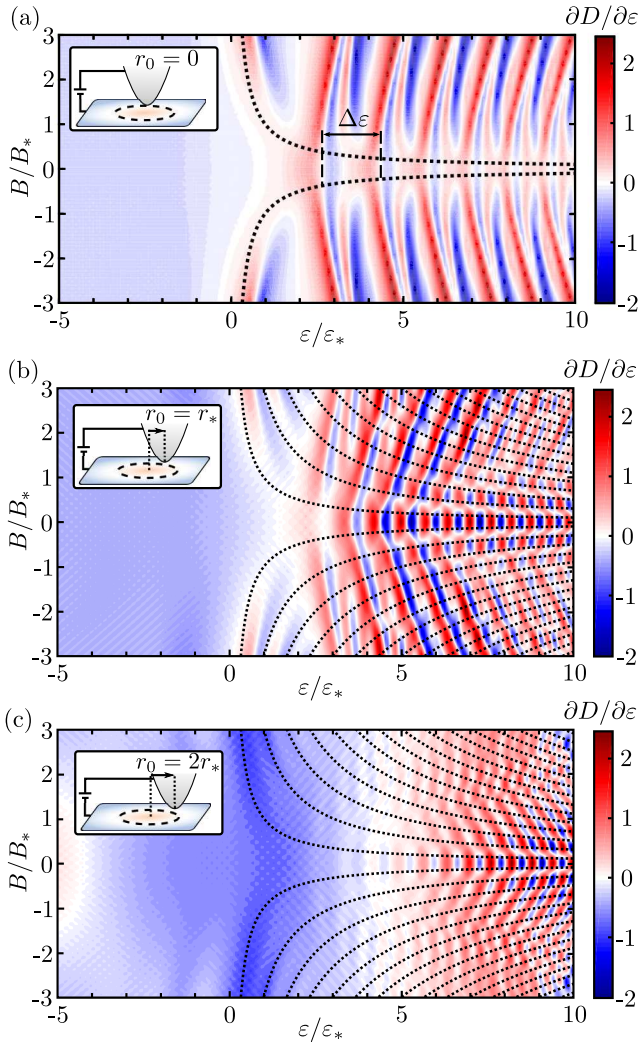


FIG. 4. Maps of the local density of states as a function of position $r_0$ for a gapless Dirac quantum dot displaying splitting of resonances in weak magnetic fields: (a) $r_0 = 0$, (b) $r_0 = r_*$, and (c) $r_0 = 2r_*$. Indicated with dotted lines is Eq.(7) for half-integer $m$. The off-centered spectral maps (b)-(c) are qualitatively different from the centered case (a) which is sensitive primarily to $m = \pm 1/2$ states. Characteristic units for magnetic field, $B_*$, is defined in Eq.(11). Plotted with dotted lines is Eq.(7) for half-integer $m$. To enhance spectral features, we plot in both panels the derivative of the local Density of States in Eq.(12).

that large $m$ states, which can be probed in off-centered STS measurement, are equally susceptible to the Berry phase splitting. Figure 4(b) and (c) show such spectral maps, in which the wavefunctions are probed at (b) $r_0 = r_*$ and (c) $r_0 = 2r_*$. In these cases, there is an overlap of peak splitting at different values of $B$, highlighted with fans of $B_c$ in Eq.(7) for varying $m$ (dotted lines). At a larger value of $r_0$, states with larger $m$ and $\varepsilon$ can be probed. This is indicated by a larger contrast in the local density of states induced by such states in Fig.4(b) and (c).

As shown in Fig.5, the splitting of the resonances for

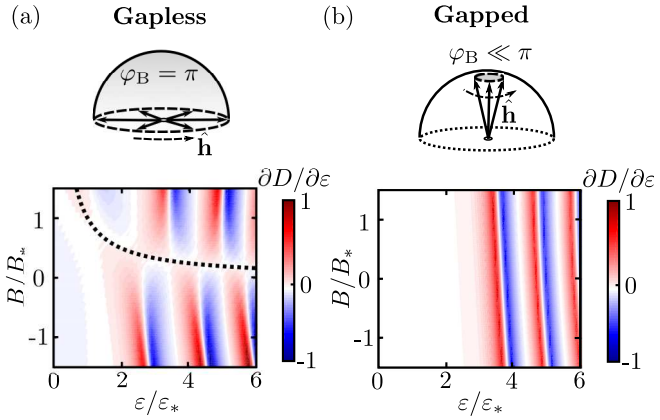


FIG. 5. Partial-$m$ contribution to the on-center density of states for quantum dots in a) gapless and b) gapped Dirac systems. The strong non-reciprocal effect induced by Berry phase disappears when a large gap $\Delta$ is opened. As a result, resonance splitting is dominated by (a) the Berry phase jump in gapless systems, and (b) orbital effects in gapped systems. The distinct behavior between (a) and (b) is shown in the partial $m = 1/2$ maps of the density of states [indicated with a dotted line is Eq.(7) with $m = 1/2$; $\Delta/\varepsilon_* = 5$ was used in (b)].

gapped systems is less prominent; in particular, splitting is dominated by the orbital contribution. Indeed, the peak splitting for the low-energy resonances in gapped Dirac systems ($\varepsilon \gtrsim \Delta$) can be quantified using a simple non-relativistic model that is valid in the limit $\Delta \gg \varepsilon_*$. In this case, expansion of the Dirac Equation in powers of $\Delta$ results in a massive Schrödinger Equation for the first spinor component $\Psi_1(\boldsymbol{r})$:

$$\left[\boldsymbol{q}^2/2\Delta + U(\boldsymbol{r}) + \Delta - eB/2\Delta\right]\Psi_1 = \varepsilon_{n,m}\Psi_1,$$
$$\varepsilon_{n,m} = \hbar\omega\left(2n + |m_-| + 1\right) - \mu_\Delta m_+ B. \tag{13}$$

Here $\varepsilon_{n,m}$ are the quantized eigenvalues, $\omega = \sqrt{2\kappa/\Delta + e^2B^2/4\Delta^2}$, and $m_\pm = m \pm 1/2$. Importantly, the orbital magnetic moment $\mu_\Delta = e\hbar v^2/2\Delta$, which is 3/2 times larger that the orbital magnetic moment of a free, massive Dirac particle at the Dirac point, induces the peak splitting observed in Fig.5(b).

### Self-consistent calculation of the potential profile

Estimates for $\kappa$ used in Eq.(8) of the main text can be obtained from a simple electrostatic model describing a biased metallic sphere proximal to the graphene plane [Fig.6(a)]. This portrays quite accurately a metallic STM tip on top of graphene, as shown in Ref.[1]. We denote $R$ the metallic sphere radius, and $d$ the sphere-graphene distance. A potential bias differential $\delta V_b$ between the sphere and graphene [see Fig.6(b)–(c)] results in a spatially varying image charge density profile given by

$$\delta n(r) \approx -\frac{e\delta V_b + \mu(r)}{4\pi e^2(d + r^2/2R)}. \tag{14}$$

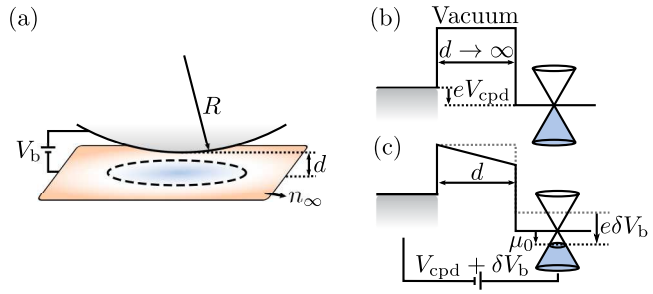


FIG. 6. (a) Schematics of the electrostatic model, showing a metallic sphere of radius $R$ separated a distance $d$ from the graphene plane. A potential bias $V_\mathrm{b}$ applied on the sphere induces a local variation of the carrier density, different from the carrier concentration density $n_\infty$ far from the sphere. (b,c) Band structure schematics showing band alignment between the metallic sphere and graphene for (b) large separation and (c) close proximity. Here $V_\mathrm{cpd}$ is the contact potential difference between graphene and the metallic sphere, $\delta V_\mathrm{b} = V_\mathrm{b} - V_\mathrm{cpd}$, and $\mu_0$ is the Fermi energy under the sphere.

Here $\delta n(r) = \mathrm{sgn}[\mu(r)]\mu(r)^2/\pi(\hbar v)^2 - n_\infty$ is the sphere-induced charge density variation on graphene, with $\mu(r)$ the Fermi energy and $n_\infty$ the gate-induced carrier density far from the center. Equation (14) is obtained from a parallel-plate capacitor model with slowly varying interplate-distance $d_\mathrm{c}(r) \approx d + r^2/2R$. Higher order terms arising due to the curvature of the electric field lines are neglected.

A straight-forward calculation yields a value of $\kappa = -\mu''(0)/2$ given by

$$\kappa = -\frac{e\delta V_\mathrm{b} + \mu_0}{2Rd\sqrt{1+|\beta|}}. \tag{15}$$

The variable $\mu_0$ is the Fermi level under the sphere, and $\beta$ is a dimensionless number:

$$\begin{aligned} \mu_0 &= \frac{(\hbar v)^2}{8e^2 d}\frac{1-\sqrt{1+|\beta|}}{\mathrm{sgn}(\beta)}, \\ \beta &= \frac{16e^2 d}{(\hbar v)^2}\left[e\delta V_\mathrm{b} - 4\pi e^2 d n_\infty\right]. \end{aligned} \tag{16}$$

Considering typical values of $R \sim 1\,\mu$m, $d \sim 5\,$nm, $\delta V_\mathrm{b} \sim 0.1\,$V and $n_\infty \sim 10^{11}\,\mathrm{cm}^{-2}$, we obtain the value of $\kappa \sim 4 \cdot 10^{-6}\,\mathrm{eV/nm}^2$ used in the main text.

## IV. DISCUSSION

Compared to previous mechansims for non-reciprocity in electronic systems, which are highly sought for in photonics and plasmonics, our realization is perhaps the first one which is inherent to Dirac materials. Indeed, Faraday and Kerr rotation, two notable examples of non-reciprocity which can be sizable in two dimensional materials such as graphene[23, 24], are also present in general semiconductor materials. The same applies to magnetoplasmonic effects, e.g. unidirectional low frequency edge modes[25–29], which are also present in generic two-dimensional structures[25].

Interestingly, the anomalous strength of the non-reciprocal effect allows to envision a new class of optical devices, such as nanoscale isolators and circulators, which are driven by Berry phase. In particular, we expect photonic effects in Dirac quantum dots to be dramatic. Indeed, electrostatic doping can, via the Pauli blocking mechanism, induce a strong and tunable electron-photon coupling. This, combined with the in situ tunability of the resonance dispersion[1], can make Dirac quantum dots critical components for miniaturizing nanophotonic systems.

We also note that our non-reciprocal effect resonates with other exotic manifestations of Berry phase predicted to occur in Dirac systems, such as Berry phase modification to exciton spectra [30, 31], optical gyrotropy induced by Berry's phase [32] and chiral plasmon in gapped Dirac systems [33, 34]. In realistic electronic systems, however, electron decoherence usually hinders observation of such subtle effects. As a result, we anticipate that readily available quantum dots states in Dirac materials enable a new and optimal setting for locally probing Berry phase physics.

Given that our predictions only rely on the Dirac nature of charge carriers, they can be tested in a wide range of materials and metamaterials. In particular, the strong dependence of resonance splitting on $\Delta$ can be explored using various systems: graphene is the prototypical material to explore the case $\Delta = 0$; graphene on top of closely-aligned hBN substrate allows to explore the case $\Delta \sim 50\,$meV [35, 36]; monolayers of transition metal dichalcogenides such as $MoS_2$ allows to explore $\Delta$ on the eV ballpark[37–39]. Furthermore, the value of $\varepsilon_*$ can also be tuned with electrostatic potential shape, as demonstrated in Ref.[1].

## SUMMARY

To summarize, quantum dots embedded in Dirac materials grant access to a new non-reciprocity mechanism originating from the Berry phase. This mechanism, which is unique to Dirac materials, leads to stronger non-reciprocity than other known mechanisms. The anomalous strength of the effect and its in situ tunability makes Dirac quantum dots an appealing platform for non-reciprocal nanophotonics. The recent introduction of Dirac quantum dots in graphene makes our predictions easily testable in on-going experiments.

## ACKNOWLEDGEMENTS

We thank M. S. Dresselhaus, J. Stroscio and B. Skinner for advice and valuable discussions, and acknowledge support by the National Science Foundation Grant No. DMR-1004147 [J.F.R.-N.] and by the Center for Excitonics, an Energy Frontier Research Center funded by the US Department of Energy, Office of Science, Basic Energy Sciences under Award No. DE-SC0001088 [LL].


## Appendix A: Computational details

To solve Eq.(10) of the main text, we use the finite difference method in the interval $0 < r < L$. The azimuthal quantum numbers are chosen in a finite range, $-M \leq m \leq M$, with $M$ large enough to represent accurately the states in the energy range of interest. In our calculations, we used a system of size $L/r_* = 10$ discretized in $N = 600$ lattice sites, with maximum azimuthal quantum number $M = 31/2$. To calculate the density of states, Eq.(12) of the main text, we approximate the delta-function $\delta(\varepsilon)$ by a Lorentzian $\delta(\varepsilon) \approx \Gamma/\pi(\varepsilon^2 + \Gamma^2)$. Here we used a broadening $\Gamma/\varepsilon_* = 0.25$, and set a Gaussian weight $\lambda_d/r_* = 0.1$ in the spatial average $\langle \ldots \rangle_{\lambda_d}$ of the wavefunctions.


[1] Y. Zhao, J. Wyrick, F. D. Natterer, J. F. Rodriguez-Nieva, C. Lewandowski, K. Watanabe, T. Taniguchi, L. S. Levitov, N. B. Zhitenev, and J. A. Stroscio, Science **348**, 672 (2015).

[2] H.-Y. Chen, V. Apalkov, and T. Chakraborty, Phys. Rev. Lett. **98**, 186803 (2007).

[3] J. Cserti, A. Pályi, and C. Péterfalvi, Phys. Rev. Lett. **99**, 246801 (2007).

[4] J. H. Bardarson, M. Titov, and P. W. Brouwer, Phys. Rev. Lett. **102**, 226803 (2009).

[5] P. G. Silvestrov and K. B. Efetov, Phys. Rev. Lett. **98**, 016802 (2007).

[6] A. Matulis, and F. M. Peeters, Phys. Rev. B **77**, 115423 (2008).

[7] J.-S. Wu, and M. M. Fogler, Phys. Rev. B **90**, 235402 (2014).

[8] M. I. Katsnelson, K. S. Novoselov, and A. K. Geim, Nat. Phys. **2**, 620 (2006).

[9] V. V. Cheianov and V. I. Fal'ko, Phys. Rev. B. **74**, 041403 (2006).

[10] M. V. Berry, Proc. R. Soc. Lond. A **392**, 45-57 (1984).

[11] G. Sundaram and Q. Niu, Phys. Rev. B **59**, 14915 (1999).

[12] A. V. Shytov, M. S. Rudner, and L. S. Levitov, Phys. Rev. Lett. **101**, 156804 (2008).

[13] M.-C. Chang and Q. Niu, J. Phys: Condens. Matter **20**, 193202 (2008).

[14] A. F. Young and P. Kim, Nat. Phys. **5**, 222-226 (2009).

[15] D. Xiao, M.-C. Chang, Q. Niu, Rev. Mod. Phys. **82**, 1959 (2010).

[16] M.-C. Chang and Q. Niu, Phys. Rev. B **53**, 7010 (1996).

[17] Z. Yu and S. Fan, Nature Photon. **3**, 9194 (2009).

[18] L. Bi, J. Hu, P. Jiang, D. H. Kim, G. F. Dionne, L. C. Kimerling, and C. A. Ross, Nat. Photon. **5**, 758-762 (2011).

[19] A. D. Stone, Physics Today **58**, 37 (2005).

[20] K. S. Novoselov, A. K. Geim, S.V. Morozov, D. Jiang, M. I. Katsnelson, I. V. Grigorieva, S. V. Dubonos, and A. A. Firsov, Nature **438**, 197-200 (2005).

[21] Y. Zhang, Y.-W. Tan, H. L. Stormer, and P. Kim, Nature **438**, 201-204 (2005).

[22] This method of quantization on the surface of an invariant tori is known as Einstein-Brillouin-Keller (EBK) quantization rule. It differs from the usual way of quantizing using closed orbits obtained from semiclassical equations of motion. The EBK method applies to completely integrable $d$-dimensional systems as well as chaotic systems. For more details, see Ref.[19].

[23] I. Crassee, J. Levallois, A. L. Walter, M. Ostler, A. Bostwick, E. Rotenberg, T. Seyller, D. van der Marel, and A. B. Kuzmenko, Nat. Phys. **7**, 48 (2011).

[24] R. Shimano, G. Yumoto, J. Y. Yoo, R. Matsunaga, S. Tanabe, H. Hibino, T. Morimoto, and H. Aoki, Nat. Commun. **4**, 1841 (2013).

[25] V. A. Volkov, and S. A. Mikhailov, Sov. Phys. JETP **67**, 1639 (1988).

[26] W. Wang, S. P. Apell, J. M. Kinaret, Phys. Rev. B **86**, 125450 (2012).

[27] I. Crassee, M. Orlita, M. Potemski, A. L. Walter, M. Ostler, Th. Seyller, I. Gaponenko, J. Chen, and A. B. Kuzmenko, Nano Lett. **12**, 2470 (2012).

[28] H. Yan, Z. Li, X. Li, W. Zhu, P. Avouris, and F. Xia, Nano Lett. **12**, 3766 (2012).

[29] I. Petković, F. I. B. Williams, K. Bennaceur, F. Portier, P. Roche, and D. C. Glattli, Phys. Rev. Lett. **110**, 016801 (2013).

[30] A. Srivastava and A. Imamoğlu, Phys. Rev. Lett. **115**, 166802 (2015).

[31] J. Zhou, W.-Y. Shan, W. Yao, and D. Xiao, Phys. Rev. Lett. **115**, 166803(2015).

[32] S. Zhong, J. Orenstein, and J. E. Moore, Phys. Rev. Lett. **115**, 117403 (2015).

[33] A. Kumar, A. Nemilentsau, K. H. Fung, G. Hanson, N. X. Fang, and T. Low, Phys. Rev. B **93**, 041413 (2016).

[34] J. C. W. Song and M. S. Rudner, PNAS **113**, 4658 (2016).

[35] B. Hunt, J. D. Sanchez-Yamagishi, A. F. Young, M. Yankowitz, B. J. LeRoy, K. Watanabe, T. Taniguchi, P. Moon, M. Koshino, P. Jarillo-Herrero, and R. C. Ashoori, Science **340**, 1427 (2013).

[36] C. R. Woods, L. Britnell, A. Eckmann, R. S. Ma, J. C. Lu, H. M. Guo, X. Lin, G. L. Yu, Y. Cao, R. V. Gorbachev, A. V. Kretinin, J. Park, L. A. Ponomarenko, M. I. Katsnelson, Y. N. Gornostyrev, K. Watanabe, T. Taniguchi, C. Casiraghi, H.-J. Gao, A. K. Geim, K. S. Novoselov, Nat. Phys. **10**, 451 (2014).

[37] A. Ramasubramaniam, Phys. Rev. B **86**, 115409 (2012).

[38] Q. H. Wang, K. Kalantar-Zadeh, A. Kis, J. N. Coleman, and M. S. Strano, Nat. Nanotech **7**, 699 (2012).

[39] X. Xu, W. Yao, D. Xiao, and T. F. Heinz, Nat. Phys. **10**, 343 (2014).